PPPL-3233 - Preprint: February 1997, UC-426

The Roles of Electric Field Shear and Shafranov Shift in Sustaining High Confinement in Enhanced Reversed Shear Plasmas on the TFTR Tokamak

E.J. Synakowski, S.H. Batha,[a] M.A. Beer, M.G. Bell, R.E. Bell, R.V. Budny, C.E. Bush,[b] P.C. Efthimion, G.W. Hammett, T.S. Hahm, B. LeBlanc, F. Levinton,[a] E. Mazzucato, H. Park, A.T. Ramsey, G. Rewoldt, S.D. Scott, G. Schmidt, W.M. Tang, G. Taylor, and M.C. Zarnstorff

Princeton Plasma Physics Laboratory, Princeton, New Jersey USA 08543

The relaxation of core transport barriers in TFTR Enhanced Reversed Shear plasmas has been studied by varying the radial electric field using different applied torques from neutral beam injection. Transport rates and fluctuations remain low over a wide range of radial electric field shear, but increase when the local E×B shearing rates are driven below a threshold comparable to the fastest linear growth rates of the dominant instabilities. Shafranov-shift-induced stabilization alone is not able to sustain enhanced confinement.

PACS numbers: 52.55.Fa, 52.25.Fi, 52.55.Dy, 52.35.Ra

[(a)] Fusion Physics and Technology, Torrance, California 90503.

[(b)] Oak Ridge National Laboratory, Oak Ridge, Tennessee 37830.

The possible role of the radial electric field in forming and sustaining transport barriers in H modes and VH modes has been discussed extensively.[1,2,3,4] TFTR Enhanced Reversed Shear (ERS)[5] and DIII-D Negative Central Shear (NCS)[6] plasmas possess transport barriers deep in the plasma core, and large values of the radial electric field E_r and its gradient have been associated with high confinement in these regimes.[7,8] However, it remains an open question whether E_r plays a causative role in reducing transport in these cases. Indeed, high core particle, energy, and momentum confinement obtained by any means will lead to increased pressures and velocities, and most likely to large values of E_r and ∇E_r.

While E_r plays a central role in proposed mechanisms for transport bifurcation and good confinement,[9] other proposals have been made in which it is not involved.[10,11] The suggestion that E_r is key in balanced-injection TFTR ERS plasmas takes the following form: central fueling and heating results in steep gradients in the plasma pressure p, which yield large gradients in E_r and the E×B flow shear.[12,13] With sufficiently large flow shear, turbulence is decorrelated. This leads to a reduction in transport, and to a further increase in ∇p and confinement. Low current density yields a large Shafranov shift Δ, and thus increased ∇p and E×B shear, as compared to plasmas with peaked current density profiles of the same stored energy. The alternative explanation for the formation of core transport barriers relies on the role of Δ itself. In Ref. 10, reduction of instability drives and the formation and sustainment of transport barriers is predicted for TFTR reversed shear plasmas as a result of favorable precession of barely trapped particles induced by large gradients in the Shafranov shift Δ'. Similar arguments were made examining ballooning-type instabilities in the plasma edge.[11] Proposals based on both E×B and Δ' effects suggest a combined picture in which growth rate reduction induced by large Δ' enables the E×B shear to be effective. In all of the above scenarios, good confinement is expected to be reinforced by the stabilization of ion-thermal-gradient turbulence from the peaking of the density profile.[14]

Results presented in this Letter indicate that E×B shear effects are necessary, and that Shafranov shift effects are not sufficient, to maintain the observed low radial transport and fluctuation levels in ERS plasmas. Experimentally, it is difficult to separate the roles of E×B shear and Δ' effects. Since steep plasma pressure gradients ∇p and large values of E_r accompany large

Shafranov shifts, a means of varying E_r independent of ∇p is required to decouple the two effects. In these experiments, ERS plasmas were generated with similar neutral beam powers and heating profiles, which fixed quantities central to Δ'-induced stabilization. However, these plasmas had different applied torques and thus varying degrees of toroidal velocity V_ϕ. For any plasma species, the radial force balance equation is given by $E_r = \nabla p/(nZe) + V_\phi B_\theta - V_\theta B_\phi$, where n is the density of the species in question, Z is the charge number, e is the electronic charge, V_θ is the poloidal rotation velocity, B_θ is the poloidal magnetic field, and B_ϕ is the toroidal field. Thus V_ϕ variations result in changes in E_r and its shear. The causative role of E_r in sustaining enhanced confinement is in part indicated by the observation that core fluctuation and transport levels increase when the E×B shear is driven below a critical level, but remain low and unchanged above that threshold. This threshold behavior is anticipated in the work of Ref. 12. Variations of amplitude and sign of V_ϕ also enable tests of the role of rotation, together with ∇p, in determining E_r's influence on enhanced core confinement,[15] and allow E_r to be altered without introducing toroidal asymmetries in the magnetic geometry.[4]

Plasmas with reverse magnetic shear were generated in the standard way[5] by heating them with modest neutral beam power (7 MW) during the period of current ramp-up. Transitions to the ERS regime were obtained during a 350 ms period of high-power beam heating (28 MW) in a balanced configuration having nearly equal power injected tangentially parallel (co) and antiparallel (counter) to the plasma current. During this period the central electron density increased rapidly due to strong core particle fueling and improved core particle confinement, reaching ~9×10^{19} m^{-3} (Fig. 1). Favorable ERS confinement was sustained for variable durations in the subsequent "postlude" period of lower-power heating (14 MW), as indicated by the continued rise in central electron density. Six neutral beam sources were used in different combinations during the postlude phase, ranging from pure co-injection to predominantly counter-injection. This procedure varied the rotation speed, and thereby the E×B shear, while maintaining a constant Shafranov shift.

The plasma pressure and pressure peakedness, total particle number, stored energy, Δ', and global energy confinement time remained nearly constant throughout the postlude period so long as the discharges remained in the ERS regime. Eventually, however, the core transport barrier was lost in some of the plasmas; they suffered a back-transition to poorer confinement, indicated most simply by the decay in central electron density. There is a clear correlation between the applied beam torque and occurrence of such a back-transition (Fig. 1). Counter-dominated, balanced, and slightly co-dominated injection sustained ERS confinement until the end of beam injection, but predominantly co-dominated injection reproducibly triggered a back-transitions. Pure co-injection yielded the earliest confinement losses. Following back-transitions, the electron particle diffusivity D_e increased by more than an order of magnitude in the region of previously-good confinement, and the electron density collapsed (Fig. 2). D_e was determined by a calculation of the particle source and electron flux Γ_e in the TRANSP code[16] and is defined by $\Gamma_e \equiv -D_e \nabla n_e + V_{ware}$, where V_{ware} is the Ware pinch. The ion thermal diffusivity (not shown) also increased in the core region following the back transition.

The correlation of back-transitions with varied applied torques at constant plasma pressure suggests that reductions in E×B shear are involved in the loss in ERS confinement. In a toroidal geometry, the gradient in the quantity E_r/RB_θ characterizes the decorrelation of turbulence, where R is the major radius. On the outer midplane, a characteristic rate for shearing turbulence can be written as $\gamma_{E\times B} = E_r/B\ [\ 1/E_r\ \partial E_r/\partial R\ -\ 1/B_\theta\ \partial B_\theta/\partial R -\ 1/R]$,[13] where B is the total magnetic field magnitude. In determining E_r, B_θ was measured with the Motional Stark Effect[17] diagnostic in the first 1.9 s of injection, when contributions from the plasma E_r to the total electric field experienced by the beam neutrals were small.[18] After this time, TRANSP calculations were used to obtain B_θ. V_ϕ and the carbon pressure p_c were measured with charge exchange recombination spectroscopy,[19] and V_θ was calculated with the NCLASS code using the neoclassical treatment of Hirshman and Sigmar.[20] In general, the $V_\phi B_\theta$ term subtracts from the ∇p_c and the $V_\theta B_\phi$ terms in the carbon force balance. Thus, increasing V_ϕ in the co-injection direction after the balanced phase leads to a reduction in E_r and its gradient. Profiles of E_r and its components from the carbon force balance equation are shown in Fig. 3 for a co-rotating plasma at two times. The first time is shortly after the 28 MW balanced phase, and the second is in the earliest stages of the back-transition. The local electron density and pressure gradients at the latter time have just begun to fall. The ∇p_c and $V_\theta B_\phi$ contributions to E_r are similar between these two times, but as a result of the increasing V_ϕ, the magnitude of E_r drops by a factor of three at r/a = 0.3. At that point, V_ϕ increased from -0.3×10^5 at 2.3 s to 1.5×10^5 m/s at 2.5 s. The $V_\phi B_\theta$ term shown in Fig. 3 is negative in the outer half of the plasma as a result of the measured counter-rotation that is present even with co-dominated injected power. NCLASS calculations indicate that the working ion V_ϕ is also counter-directed in the outer half of the plasma. TRANSP analysis shows that this is consistent with the presence of a counter-directed torque, established by a radial current of thermal particles that arises to preserve ambipolarity in response to ripple loss of about 10% of the beam ions. Regarding V_θ, measured differences in E_r in supershots with different applied torques are consistent with V_θ being driven primarily by neoclassical processes included in NCLASS, including strong poloidal damping.[18] However, large pressure gradients raise concern regarding violation of the usual size ordering assumed in neoclassical theory. Because the trapped orbit widths of carbon ions are small compared to the electric field and pressure gradient scale lengths, this ordering is not violated for this impurity. The pressure gradient scale length λ_p is 10 - 20 times the trapped carbon orbit size λ_c for r/a > 0.2, without considering the influence of orbit squeezing.[21] Squeezing effects reduce the orbit size by roughly 50% for r/a < 0.2, leading to $\lambda_p/\lambda_c > 10$ for all radii. Orbit squeezing is included in the NCLASS calculations using an approximate method.[22] Since large values of dE_r/dr change the carbon ion collisionality [Ref. 22], the predictions of V_θ and thus E_r are modified somewhat for r/a < 0.25 (Fig. 3). Such physics issues surrounding the V_θ evaluation have motivated the development of a diagnostic aimed at measuring this quantity directly.[23]

The pressure remains peaked in the region where the maximum linear growth rate $\gamma_{\rm lin}^{\rm max} < \gamma_{E\times B}$ (Fig. 4). The pressure collapses when $\gamma_{E\times B}$ is driven by rotation below a critical value comparable to $\gamma_{\rm lin}^{\rm max}$ in the core, indicating that E×B shear is necessary to sustain enhanced confinement. $\gamma_{\rm lin}^{\rm max}$ was calculated with a gyrofluid treatment that includes the role of Δ', but excludes the effects of E×B shear.[24] In these plasmas, modes are expected to become unstable primarily by the trapped electron precession resonance. In the co-dominated postlude plasmas, the loss of core stored energy occurs at different times but at comparable values of $\gamma_{E\times B}$, again indicating that E×B shear is necessary to maintain low transport (Fig. 5). The causative role of

E×B shear is further emphasized by the fact that reductions in $\gamma_{E\times B}$ clearly precede back-transitions, while all other plasma quantities, including Δ', are constant or nearly constant.

Increases in core local fluctuation levels, measured from reflectometry,[8] are correlated with increases in local transport coefficients in plasmas with back-transitions (Fig. 6). In addition, transport coefficients and fluctuation levels remain low until $\gamma_{E\times B}$ falls below a critical vaue that is comparable to the local value of γ_{lin}^{max} . The insensitivity of transport and fluctuations to variations in $\gamma_{E\times B}$ above a threshold value, and the similar magnitude of $\gamma_{E\times B}$ and γ_{lin}^{max} at the onset of increased transport and fluctuations is consistent with expectations from Ref. 12. There, nonlinear simulations of ion drift-wave-type turbulence indicate that suppression of turbulence-induced transport should be complete when $\gamma_{E\times B} \sim \gamma_{lin}^{max}$. While the fact that $\gamma_{lin}^{max}/\gamma_{E\times B} \sim 1/2 - 1$ at the onset of turbulence is suggestive, the more important point is that the predicted threshold character of turbulence suppression is observed. In fact, variations with plasma condition in $\gamma_{lin}^{max}/\gamma_{E\times B}$ at the onset of suppression are found in both experiments and simulations. It was suggested in Ref. 12 that parametric dependencies may influence the value of $\gamma_{lin}^{max}/\gamma_{E\times B}$ at that time. There, variations of a factor of two in this ratio were observed. Changes in $\gamma_{lin}^{max}/\gamma_{E\times B}$ at the start of enhanced confinement of more than a factor of two were also observed in recent ERS experiments in which the toroidal field was varied.[25] Finally, equating γ_{lin}^{max} with the natural turbulence decorrelation rate is an approximation. The latter is the quantity more appropriately compared to the shearing rate,[2] but it is not readily evaluated. These observations point to the need for study with respect to the identification of the most relevant shear suppression criterion and its underlying dependencies.

The fluctuation amplitude increases gradually as $|\gamma_{E\times B}|$ decreases, suggesting that the smaller values of $|\gamma_{E\times B}|$ are effective in suppressing the turbulence at least partially. Note also that when transport coefficients are near a maximum, $|\gamma_{E\times B}|$ is near its local minimum value. For the plasma with co-only injection in the postlude (Fig 6(a)), transport coefficients and fluctuation levels begin to fall again after 2.6 s. After this time, the $\gamma_{E\times B}$ profile broadens and becomes dominated by gradients in V_ϕ rather than ∇p, indicating that E×B shear from rotation drive may be reducing turbulence, as has been suggested for DIII-D NCS [8] and VH-mode plasmas.[4]

Without consideration of E×B shear, the fact that back-transitions occur in plasmas with heating, pressure, and Δ' profiles that are similar until the back-transition to those of plasmas without back-transitions indicates that Δ' effects alone are not sufficient to maintain enhanced confinement. Gyrokinetic simulations[26] indicate that the velocity shears in these plasmas are far below those required to excite rotationally driven instabilities[27,28] which might cause a loss in confinement. They also indicate that stabilizing influences of V_ϕ shear are not significant here.

While Δ' is not sufficient to maintain reduced transport in the absence of E×B shear, it may still be necessary. E×B shear suppression may benefit from the reduced growth rates that result from Δ' effects. Growth rates calculated including Δ' effects are a factor of two smaller than those obtained excluding these effects. However, the gradual increase of fluctuations and transport with decreasing $|\gamma_{E\times B}|$ indicates that some reductions in transport might be expected for plasmas in which $|\gamma_{E\times B}|$ is large but where growth rates have not had the benefit of significant Δ'-induced reduction. As a result, the steep pressure gradients in TFTR supershots and accompanying large gradients in E_r may produce some reduction in turbulence-driven transport.[29,30] Differences in E×B shear from different degrees of V_ϕ may explain also many trends in isotope scaling studies, even in L mode, on TFTR.[31]

The authors wish to express their appreciation for the efforts and dedication of the TFTR staff and engineers, particularly those involved in tokamak and neutral beam operations. Thanks are due to P.H. Diamond (UCSD) for fruitful discussions, and to W. Houlberg (ORNL) for making the NCLASS code available. The encouragement of R.J. Hawryluk, K.M. McGuire, and D.W. Johnson is greatly appreciated. This work was supported by DoE Grant No. DE-AC02-76-CH-03073.

[1] R. Taylor, *et al.*, Phys. Rev. Lett. **63**, 2365 (1989).
[2] H. Biglari, P.H. Diamond, and P.W. Terry, Phys. Fluids B **2**, 1 (1990).
[3] K. Burrell *et al.*, Phys. Plasma **1**, 1536 (1994).
[4] R. LaHaye *et al.*, Nucl. Fusion **35**, 988 (1995).
[5] F. Levinton *et al.*, Phys. Rev. Lett. **75**, 4417 (1995).
[6] E. Strait *et al.*, Phys. Rev. Lett. **75**, 4421 (1995).
[7] L. Lao *et al.*, Phys. Plasmas **3**, 1951 (1996).
[8] E. Mazzucato *et al.*, Phys. Rev. Lett. **77**, 3145 (1996).

[9] P.H. Diamond *et al.*, Phys. Rev. Lett., in press.
[10] M.A. Beer and G.W. Hammett, Bull. Am. Phys. Soc. **40**, 1733 (1995).
[11] J.F. Drake *et al.*, Phys. Rev. Lett **77**, 494 (1996)
[12] R.E. Waltz *et al.*,, Phys. Plasmas **1**, 2229 (1994).
[13] T.S. Hahm and K.H. Burrell, Phys. Plasmas **2**, 1648 (1995).
[14] S. Parker, Phys. Plasmas **3**, part II, 1959 (1996).
[15] G.M. Staebler, R.E. Waltz, and J.C. Wiley, General Atomics Report GA-A22303, May 1996.
[16] R. Budny *et al.*, Nucl. Fusion **32**, 429 (1992).
[17] F. Levinton *et al.*, Phys. Rev. Lett. **63**, 2060 (1989).
[18] M.C. Zarnstorff *et al.*, accepted for publication in Phys. Plasmas.
[19] B.C. Stratton *et al.*, in *Proceedings of the IAEA Technical Committee Meeting on Time Resolved Two- and Three-Dimensional Plasma Diagnostics, Nagoya, Japan* (International Atomic Energy Agency, Vienna, 1991), p. 78.
[20] S.P. Hirshman and D.J. Sigmar, Nucl. Fus. **21**, 1079 (1981).
[21] H.L. Berk and A.A. Galeev, Phys. Fluids **10**, 441 (1967).
[22] K.C. Shaing, C.T. Hsu, and R.D. Hazeltine, Phys. Plasmas **10**, 3365 (1994).
[23] R.E. Bell, *et al.*, Bull. Am. Phys. Soc. **41**, 1378 (1996).
[24] M. A. Beer, Ph. D. thesis, Princeton University (1995)
[25] F. Levinton *et al.*, to appear in *Proceedings of the Sixteenth IAEA Conference on Plasma Physics and Controlled Nuclear Fusion Research, Montreal, 1996* (International Atomic Energy Agency, Vienna)
[26] G. Rewoldt, W.M. Tang, and R.J. Hastie, Phys. Fluids **30**, 807 (1987).
[27] N. Mattor and P.H. Diamond, Phys. Fluids. **31**, 1180 (1988)
[28] M. Artun, W.M. Tang, and G. Rewoldt, Phys. Plasmas 2, 3384 (1995)
[29] D. Ernst, Ph. D. thesis, MIT, 1997.
[30] C.E. Bush *et al.*, to be published in Proceedings of the 12th International Conference on Plasma Surface Interactions in Controlled Fusion Devices, J. Nucl. Mat., 1996.
[31] S.D. Scott *et al.*, to appear in *Proceedings of the Sixteenth IAEA Conference on Plasma Physics and Controlled Nuclear Fusion Research, Montreal, 1996* (International Atomic Energy Agency, Vienna)

Figure captions

Fig. 1 The central electron density time evolution. Curves are labeled according to the difference on co- vs. counter-injected power, P_{co} - P_{ctr}, divided by the total injected power P_{tot}. The shaded region indicates schematically the neutral beam heating waveform. The plasmas studied had a major radius of 2.60 m, a minor radius of 0.95 m, a toroidal magnetic field of 4.6 T, and a maximum plasma current of 1.6 MA.

Fig. 2 (a) Profiles of the electron density at four times for a plasma that is co-dominated in the postlude [$(P_{co}$-$P_{ctr})/P_{tot}$ = 0.62]. (b) Radial profiles of D_e for the same plasma. Profiles of D_e for the other plasmas during the ERS period are similar to the profiles shown for 2.3 - 2.4 s

Fig. 3 (a) Radial profile of E_r for the plasma discussed in Fig. 2 ([$(P_{co}$-$P_{ctr})/P_{tot}$ = 0.62], and the contributions from the components of the carbon force balance equation at 2.3 s. The shaded regions represent the difference in the V_θ term and the net E_r calculated if orbit squeezing effects are ignored. (b) Same as (a), but for 2.5 s, in the early stages of confinement loss.

Fig. 4 Profiles of shearing rate and total plasma pressure for a counter-dominated plasma [$(P_{co}$-$P_{ctr})/P_{tot}$ = -0.4] (a,b), and one of the co-dominated plasmas [$(P_{co}$-$P_{ctr})/P_{tot}$ = 0.62] (c,d). In the co-dominated case, the plasma pressure is unchanged until $\gamma_{E\times B}$ falls well below γ_{lin}^{max}).

Fig. 5 (a) The stored energy, integrated out to r/a = 0.3 for plasmas with and without back transitions. This location is near the radius of maximum $\gamma_{E\times B}$ before the back-transition, and is near the boundary of the region of low fluctuations (Ref. 8). (b) $\gamma_{E\times B}$ at r/a = 0.3. Also shown is the linear growth rate γ_{lin}^{max} for the co-dominated case with the latest back-transition [$(P_{co}$-$P_{ctr})/P_{tot}$ = 0.62]. Growth rates for the other plasmas during their 14 MW postlude ERS phases are comparable. (c) The gradient in the Shafranov shift, Δ', at r/a= 0.3.

Fig. 6 The effective particle diffusivity D_e, and measured fluctuation amplitudes at r/a = 0.3 for plasmas with (a) all co-injection [$(P_{co}-P_{ctr})/P_{tot} = 1.0$] , (b) predominantly co-injection [$(P_{co}-P_{ctr})/P_{tot} = 0.62$], and (c) balanced injection [$(P_{co}-P_{ctr})/P_{tot} = 0.0$] in the postlude.

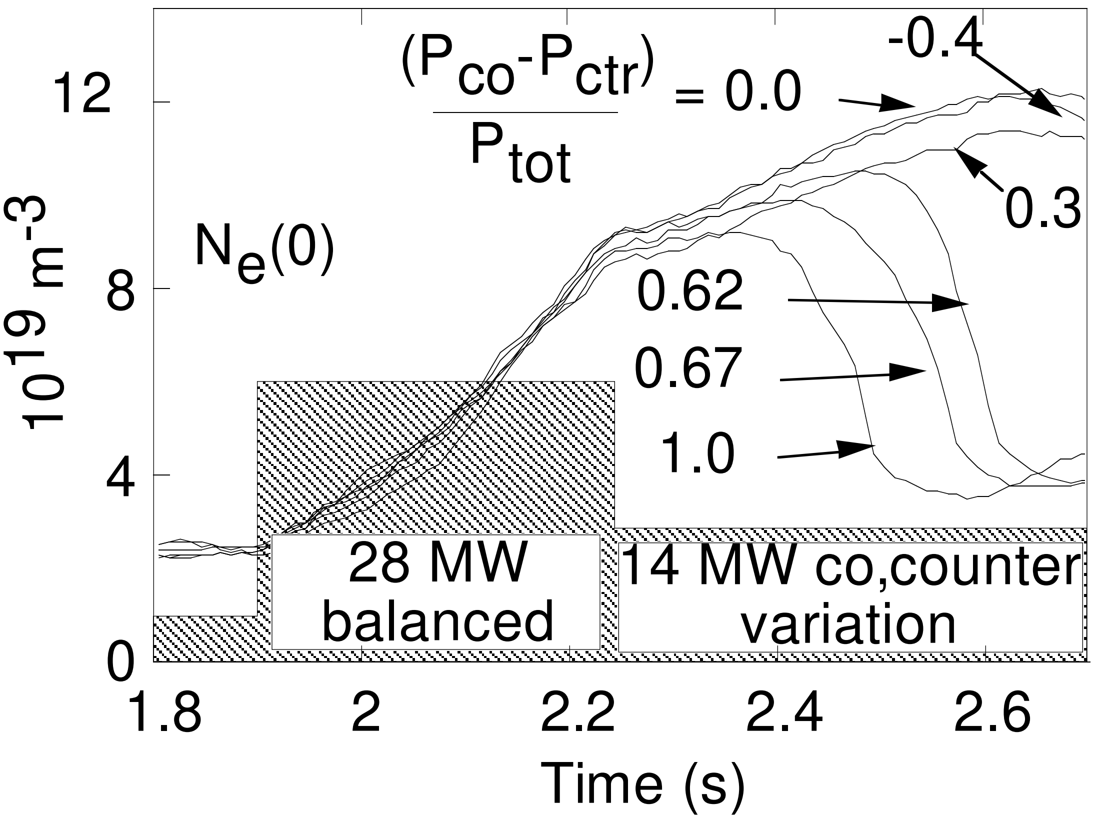

$(P_{co}-P_{ctr})$
P_{tot}
= 0.0
-0.4
0.3
$N_e(0)$
0.62
0.67
1.0
$10^{19}m^{-3}$
12
8
4
0
28 MW
balanced
14 MW co,counter
variation
1.8
2
2.2
2.4
2.6
Time (s)

Figure 1

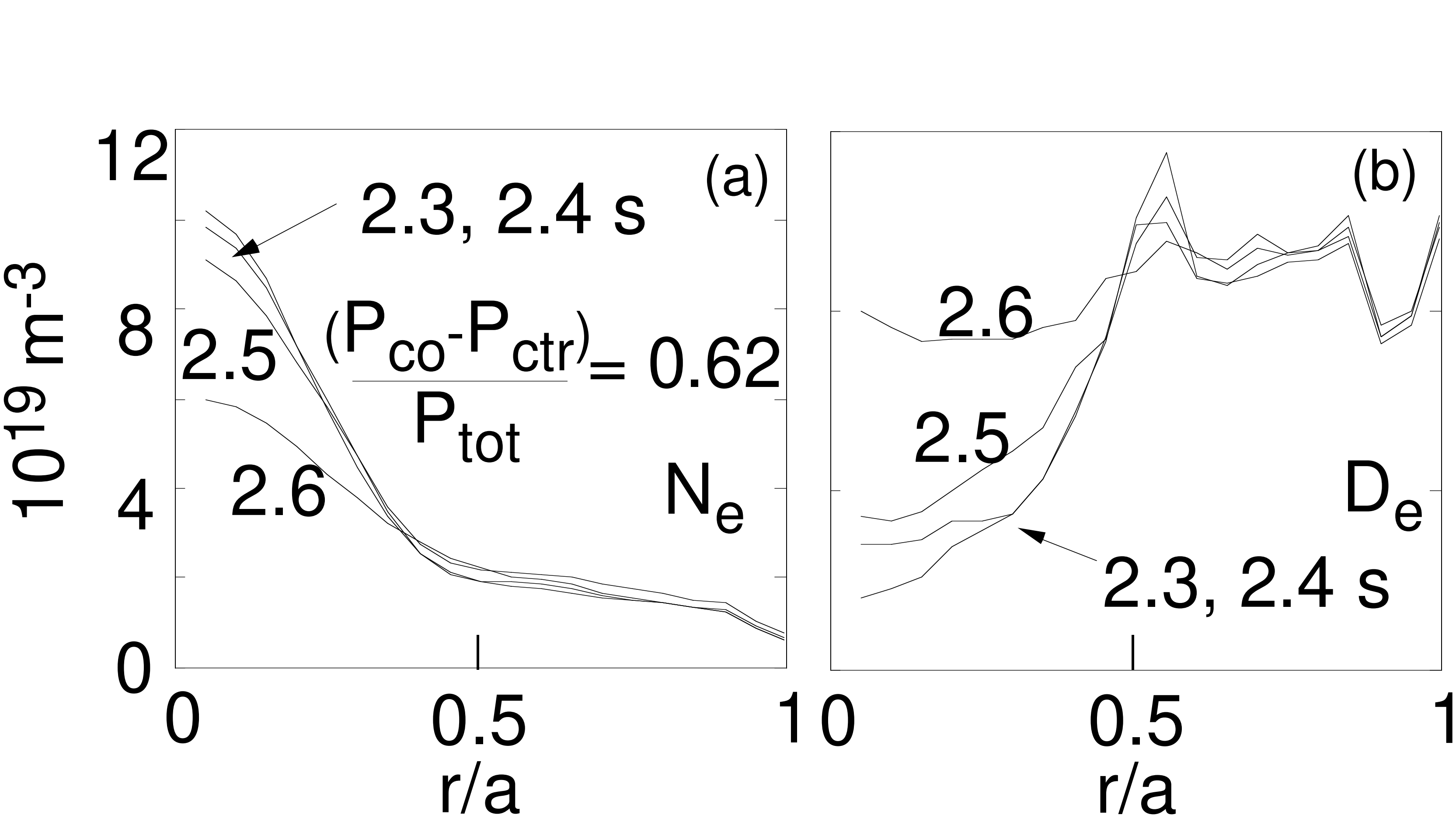
12
8
4
0
$10^{19}\,m^{-3}$
(a)
2.3, 2.4 s
$\frac{(P_{co}-P_{ctr})}{P_{tot}} = 0.62$
2.5
2.6
N_e
0
0.5
1
r/a
(b)
2.6
2.5
D_e
2.3, 2.4 s
0
0.5
1
r/a

Figure 2

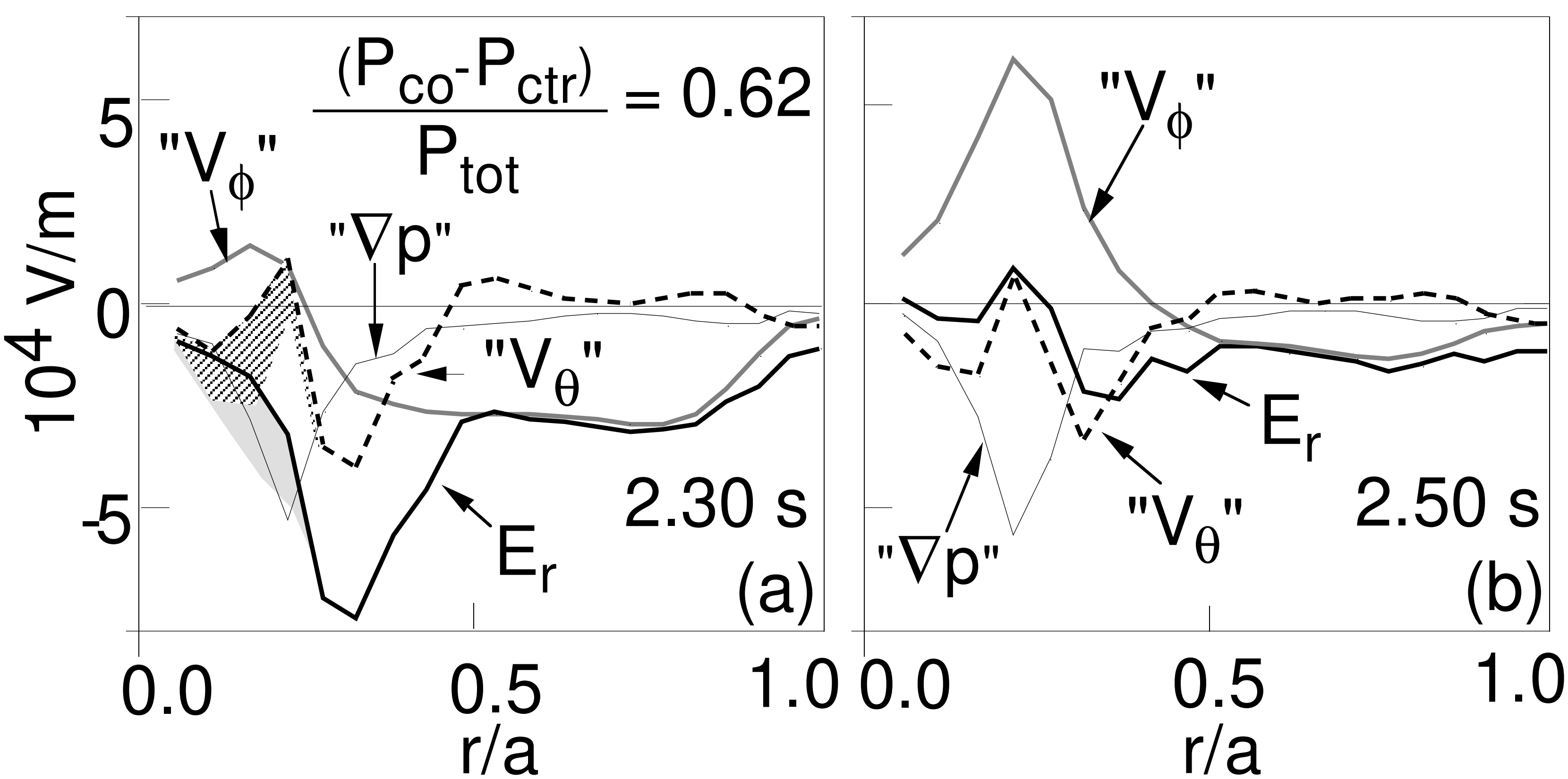

$\frac{(P_{co}-P_{ctr})}{P_{tot}} = 0.62$
"V_ϕ"
"∇p"
"V_θ"
E_r
2.30 s
(a)
"V_ϕ"
E_r
"V_θ"
"∇p"
2.50 s
(b)
10^4 V/m
5
0
-5
0.0
0.5
1.0
r/a

Figure 3

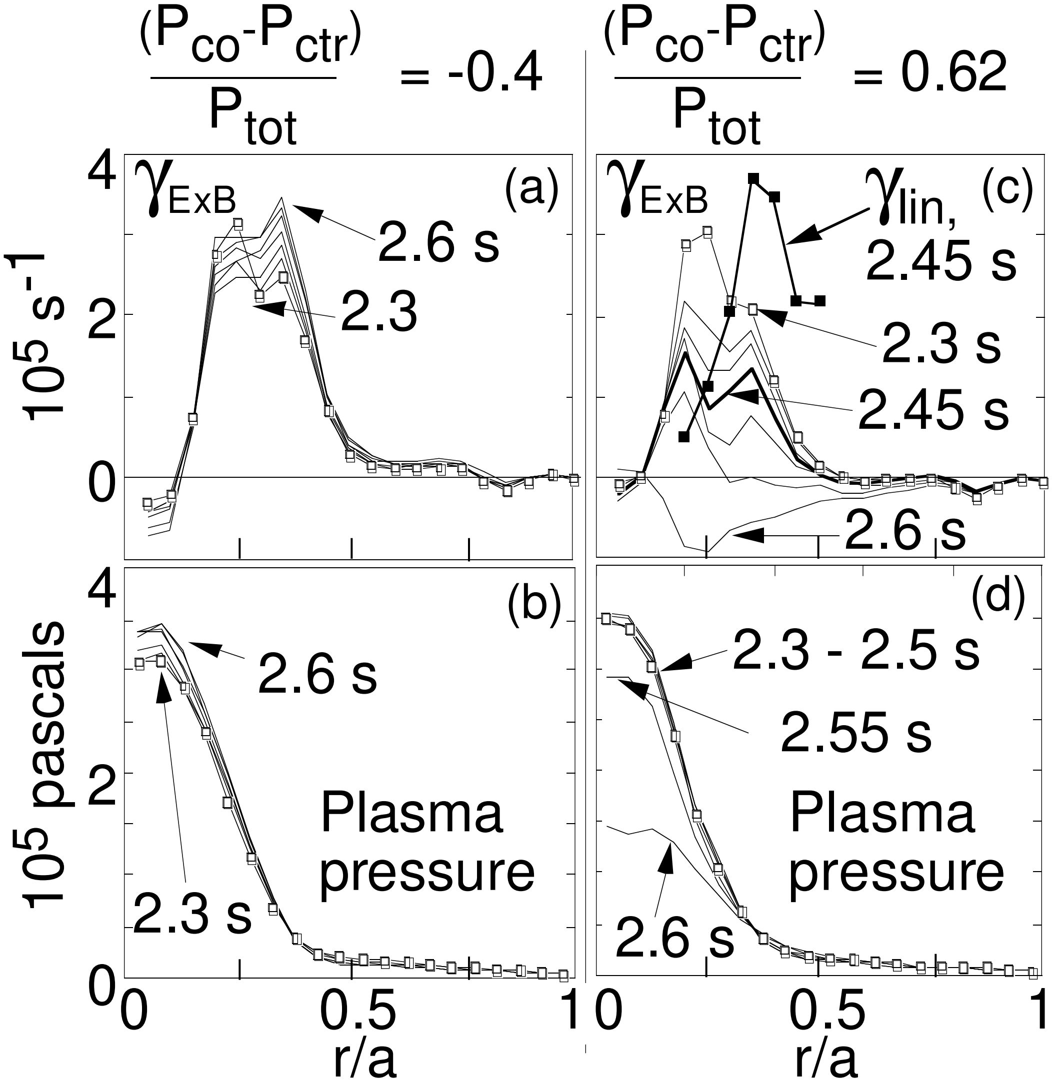

$\frac{(P_{co}-P_{ctr})}{P_{tot}}$ = -0.4
$\frac{(P_{co}-P_{ctr})}{P_{tot}}$ = 0.62
γ_{ExB}
(a)
2.6 s
2.3
10^5 s^{-1}
γ_{ExB}
γ_{lin}, 2.45 s
(c)
2.3 s
2.45 s
2.6 s
(b)
2.6 s
10^5 pascals
Plasma pressure
2.3 s
(d)
2.3 - 2.5 s
2.55 s
Plasma pressure
2.6 s
r/a
r/a

Figure 4

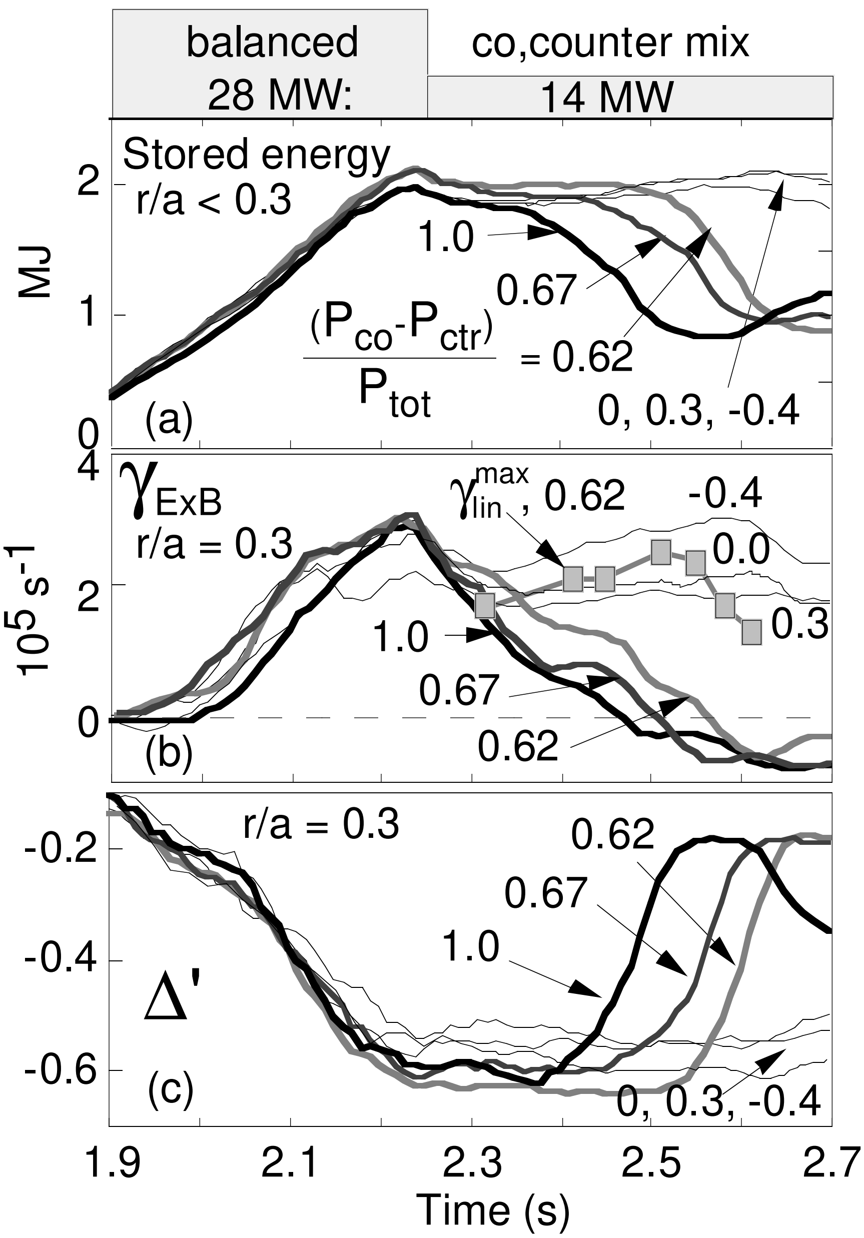
balanced
28 MW:
co,counter mix
14 MW
Stored energy
r/a < 0.3
MJ
1.0
0.67
(Pco-Pctr) / Ptot = 0.62
0, 0.3, -0.4
(a)
γExB
r/a = 0.3
10^5 s^-1
γlin max, 0.62
-0.4
0.0
0.3
1.0
0.67
0.62
(b)
r/a = 0.3
0.62
0.67
1.0
Δ'
0, 0.3, -0.4
(c)
1.9
2.1
2.3
2.5
2.7
Time (s)

Figure 5

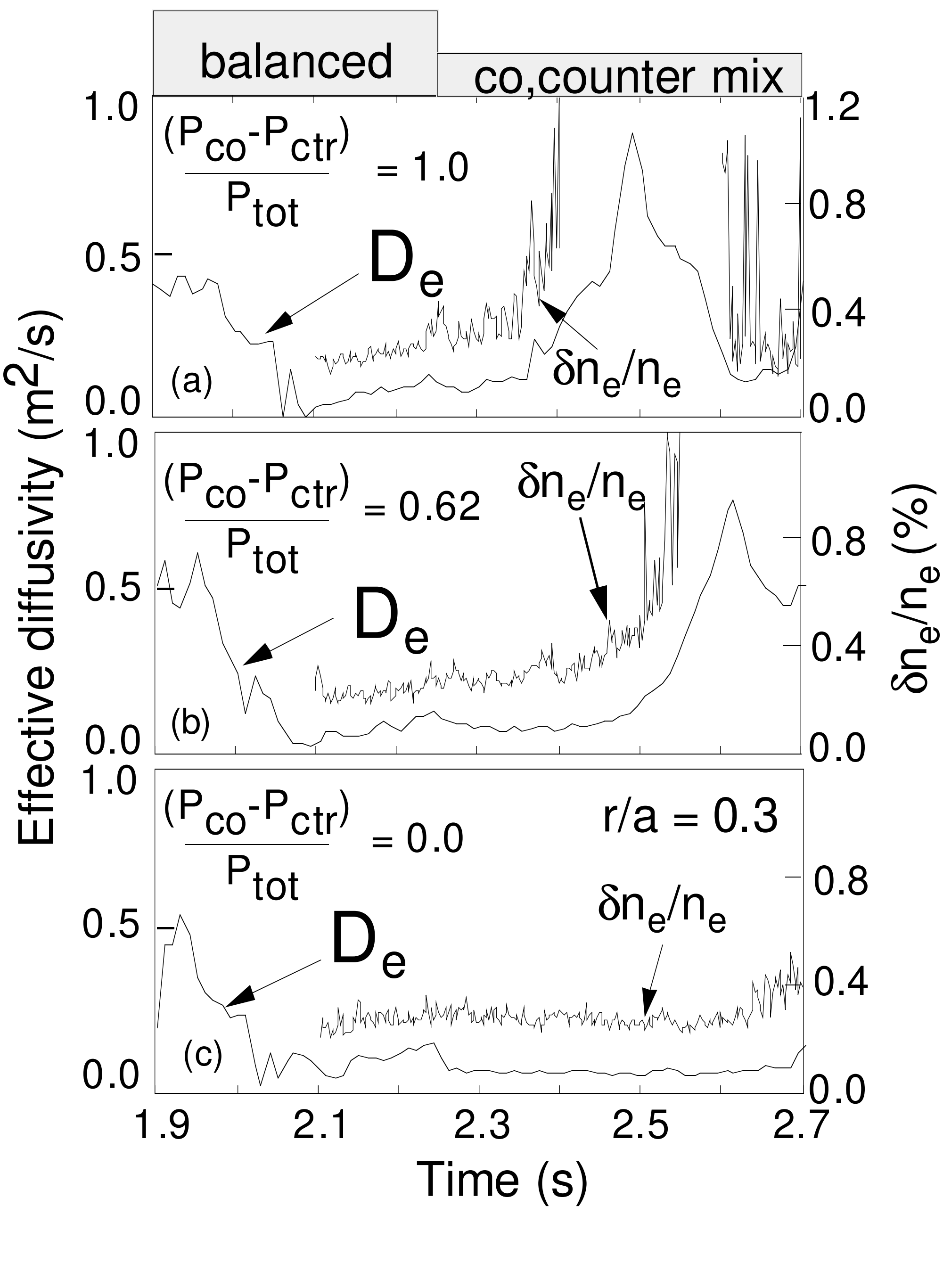

balanced
co,counter mix
Effective diffusivity (m2/s)
δne/ne (%)
(Pco-Pctr)/Ptot = 1.0
De
δne/ne
(a)
(Pco-Pctr)/Ptot = 0.62
δne/ne
De
(b)
(Pco-Pctr)/Ptot = 0.0
r/a = 0.3
δne/ne
De
(c)
Time (s)

Figure 6